



Kinetic modeling of sonocatalytic degradation of an azo dye using synthesized zinc-iron nanolayered double hydroxide

Lale Samaei^a, Alireza Khataee^{a,b,*}, Samira Arefi-Oskoui^a

^aResearch Laboratory of Advanced Water and Wastewater Treatment Processes, Department of Applied Chemistry, Faculty of Chemistry, University of Tabriz, 51666–16471 Tabriz, Iran, Tel. +98 413 3393165; Fax: +98 413 3340191; email: a_khataee@tabrizu.ac.ir (A. Khataee)

^bDepartment of Materials Science and Nanotechnology Engineering, Faculty of Engineering, Near East University, 99138 Nicosia, North Cyprus, Mersin 10, Turkey

Received 22 August 2018; Accepted 17 January 2019

ABSTRACT

The removal of bordeaux red B as an azo dye in the presence of zinc-iron nanolayered double hydroxide was investigated under ultrasonic irradiation to propose a proper kinetic model. A facile co-precipitation method was used for preparing the zinc-iron nanolayered double hydroxide and the as-synthesized nanolayered double hydroxide was characterized using UV–Vis diffuse reflection spectroscopy (UV–Vis diffuse reflection spectroscopy), X-ray diffraction and scanning electron microscopy techniques. The effect of the sonocatalyst concentration and initial bordeaux red B concentration were studied in order to discover the kinetic characteristics of the sonocatalytic degradation of bordeaux red B. Considering the intrinsic elementary reactions of sonocatalytic degradation of bordeaux red B, a novel kinetic model was developed and validated. The proposed kinetic model revealed the dependence of the apparent first-order rate constant on the main operational parameters. The obtained results revealed that the developed model was in a good agreement with experimental data with a good correlation coefficient ($R^2 > 0.975$).

Keywords: Kinetic modeling; Zinc-iron nanolayered double hydroxide; Sonocatalytic degradation; Intrinsic elementary reactions

1. Introduction

In recent decades, synthetic organic dyes have been widely used in various industries including leather, paper, cosmetic and textile [1,2]. Disposal of great amount of colored and toxic effluents which are generally harmful and resistant to biological degradation causes hazardous contamination of surface and ground water [1,3,4].

Azo dyes containing one or more azo bonds ($-N=N-$) in their structure are the most important group of dyes used in the textile industries. These dyes are carcinogenic and their presence in aqueous environment decreases the light penetration, resulting in decelerating the self-purification of streams [5,6].

Nowadays, the advanced oxidation processes (AOPs), known as efficient methods for the removal of organic pollutants, have been widely applied in wastewater treatment [6,7]. Among the AOPs, ultrasonic process is a promising method for the wastewater remediation that has received great attention in recent years [8,9]. During ultrasonic process, cavitation phenomenon including nucleation, growth and collapse of the bubbles caused by ultrasound waves produces extremely high temperature (5,000 K) and pressure (1,000 bar) inside the bubble [10]. In this process, the high temperature adjacent the bubbles causes thermal dissociation of water molecules which produces hydroxyl radicals as one of the most powerful oxidizing radicals. Easy management and high degradation efficiency are of the main advantages of the ultrasonic process [11–13]. However, this process is

* Corresponding author.

time and energy consuming and complete mineralization rarely occurs. To overcome these limitations, the ultrasonic method can be merged with sonocatalyst. Among the different materials used as sonocatalyst, semiconductors have got great attention in this field [8,14].

Layered double hydroxides (LDHs) are a class of lamellar materials comprised of positively charged host layers with an interlamellar area containing anions and solvation molecules [15]. General formula of LDH compounds is $[M_{1-x}^{2+}M_x^{3+}(\text{OH})_2]^{x+}[A_{x/m}]^{n-}.m\text{H}_2\text{O}$, in which M^{2+} and M^{3+} represent divalent metal cation (e.g., Ni^{2+} , Zn^{2+} , Fe^{2+} or Cu^{2+}) and trivalent metal cation (e.g., Fe^{3+} , Mn^{3+} , Al^{3+} or Ga^{3+}), respectively. A^{n-} represents organic or inorganic anion by negative charge of n ; and m shows the number of water molecules in the interlayer region. In this formula, the value of x is determined by molar ratio of $M^{3+}/M^{2+}+M^{3+}$ [16–18]. Recently, layered double hydroxides have received notable considerations owing to their significant structural features such as considerable thermal stability, great anion-exchange ability and large surface area [19]. In addition, LDHs have been applied as catalyst in different processes such as photo-degradation of organic pollutants and complete destruction of organic compounds [20,21].

Studying the mechanism and kinetics of sonocatalytic process is vital to scale up the sonocatalytic degradation and also to design high efficient reactors for this process. According to previous reports, sonocatalytic oxidation of various organic compounds has been modeled by pseudo-first-order kinetics (Eq. (1)) [9,22] and Langmuir–Hinshelwood equation (Eq. (2)) [23,24] as a function of irradiation time and contaminant concentration, respectively.

$$r = -\frac{dC}{dt} = k_{\text{app}}C \Rightarrow \ln\left(\frac{C}{C_0}\right) = -k_{\text{app}}t \quad (1)$$

$$r = \frac{k_r k_s C}{1 + k_s C_0} \quad (2)$$

where r is the reaction rate ($\text{g L}^{-1} \text{min}^{-1}$), C_0 and C show the concentration of contaminant in initial and after t time of reaction, respectively. In the mentioned formulas, k_r is the reaction rate constant ($\text{g L}^{-1} \text{min}^{-1}$), k_s is the adsorption rate constant of goal compound (L g^{-1}), and k_{app} is the apparent pseudo-first-order rate constant [25–28].

This study aims at investigating the reaction kinetics of sonocatalytic degradation of bordeaux red B as an azo dye by applying zinc-iron nanolayered double hydroxide. For this purpose, intrinsic elementary reactions which contain comprehensive concept of the method and effects of operational parameters are considered to develop a kinetic model [29]. A facile co-precipitation method was used for synthesizing zinc-iron nanolayered double hydroxide, and the as-synthesized nanolayered double hydroxide was characterized using scanning electron microscopy (SEM), X-ray diffraction (XRD) and UV–Vis diffuse reflection spectroscopy techniques. To the best of our knowledge, investigating intrinsic kinetic model for sonocatalytic activity of the zinc-iron nanolayered double hydroxide has not been reported previously. A novel kinetic model was developed based on intrinsic elementary reactions for sonocatalytic process.

2. Experimental

2.1. Reagents and materials

Zinc chloride (ZnCl_2), ferric chloride hexahydrate ($\text{FeCl}_3 \cdot 6\text{H}_2\text{O}$) and sodium hydroxide (NaOH) were provided by Merck, Germany. Bordeaux red B was purchased from Shimi Boyaksaz Co., Iran. Table 1 reports the main characteristics of bordeaux red B.

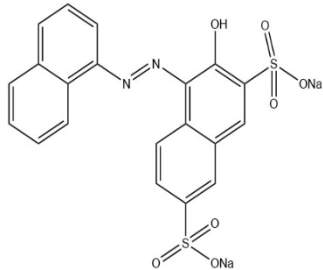
2.2. Synthesis of zinc-iron nanolayered double hydroxide

The zinc-iron nanolayered double hydroxide was synthesized through co-precipitation method. In a typical synthesis process, 0.001 mol of ferric chloride hexahydrate and 0.003 mol of zinc chloride were dissolved in deionized water under N_2 atmosphere. NaOH solution with concentration of 3 mol L^{-1} was added dropwise to the prepared solution. The prepared suspension was stirred under N_2 atmosphere for 24 h. The synthesized nanolayered double hydroxide crystallites were washed with deionized water after collection. Eventually, the prepared nanolayered double hydroxides were dried at 50°C .

2.3. Characterization methods

A SEM was used to investigate the morphology of the prepared nanolayered double hydroxide by using a TESCAN, MIRA3 (Czech Republic).

Table 1
Characteristics of bordeaux red B

Dye	Chemical structure	Molecular formula	Color index number	λ_{max} (nm)	M_{tr} (g mol^{-1})
Bordeaux red B		$\text{C}_{20}\text{H}_{12}\text{N}_2\text{Na}_2\text{O}_7\text{S}_2$	16,180	$511 \pm 2 \text{ nm}$	502.435

XRD measurement was performed at room temperature using a Philips X-ray diffraction PW1730 diffractometer (Netherlands) Cu K α radiation ($\lambda = 1.54065 \text{ \AA}$), at an accelerating voltage of 40 kV and emission of current of 30 mA.

An UV–Vis spectrophotometer (Sinco Co model S 4100, Korea) was used to evaluate the band gap of synthesized zinc-iron nanolayered double hydroxide in the range of 200–800 nm.

2.4. Experimental conditions for kinetic study of the degradation process

In order to investigate the effect of the sonocatalyst dosage and initial dye concentration on the kinetic characteristics of the reaction, the sonocatalytic degradation of bordeaux red B was investigated in an ultrasonic bath apparatus. For this experiment, 100 mL of bordeaux red B solution with a certain amount of sonocatalyst was irradiated in the ultrasonic bath with frequency of 50 Hz and 300 W output power. The experiments were conducted in the dark to omit the influence of the photolysis and photocatalysis. Every 15 min, sampling of the dye solution was performed from the reactor and the remaining concentration of dye was measured using an UV–Vis spectrophotometer at a maximum wavelength of 550 nm. The degradation efficiency (%) of bordeaux red B via sonocatalytic process was determined using Eq. (3):

$$\text{Degradation efficiency (\%)} = \frac{C_0 - C_t}{C_0} \times 100 \quad (3)$$

where C_0 and C_t represent the absorbance of the dye solution in initial time and t time, respectively.

3. Results and discussion

3.1. Characterization of synthesized zinc-iron nanolayered double hydroxide

The crystallite structure of the synthesized zinc-iron nanolayered double hydroxide was studied using XRD analysis. As can be observed in Fig. S1, the XRD diffraction peaks centered at 2θ values of 11.94° , 20.64° , 23.84° , 28.94° , 31.09° , 33.19° , 35.39° , 59.09° and 60.34° which are related to the 001, 002, 003, 110, 111, 112, 113, 031 and 032 planes reflection demonstrated that nanolayered double hydroxide was successfully synthesized [30]. The mean crystallite size of the prepared sample (D) was calculated to be 13 nm using Debye-scherrer's formula based on the sharpest peak (11.8°) [31].

The morphology of the as-synthesized zinc-iron nanolayered double hydroxide was investigated using SEM analysis. SEM images shown in Fig. 1 demonstrate that nanosheets with approximate width diameter of 32 nm were synthesized.

Band gap value of zinc-iron nanolayered double hydroxide was determined using UV–Vis diffuse reflectance spectra analysis. The optical absorption near the band gap of the sonocatalyst can be determined according to Eq. (4) [32].

$$\alpha h\nu = K(h\nu - E_g)^{0.5} \quad (4)$$

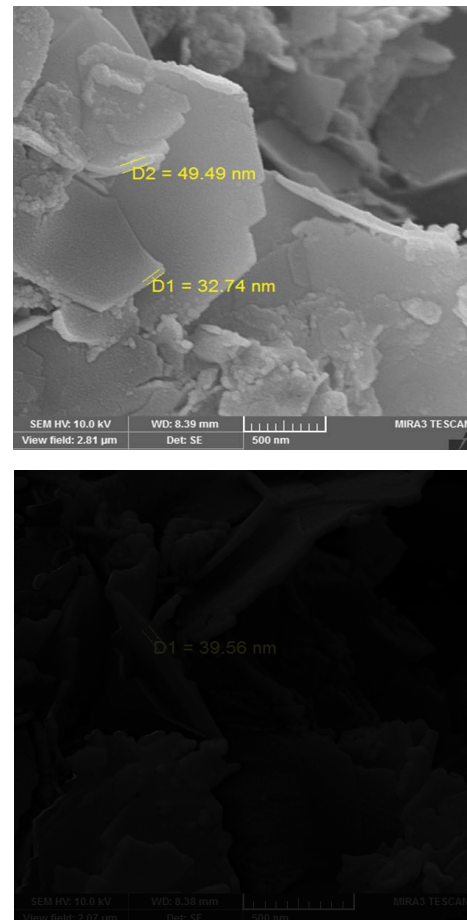


Fig. 1. SEM images of the zinc-iron nanolayered double hydroxide.

where α and $h\nu$ demonstrate the absorption coefficient and photon energy (eV), respectively. Moreover, K and E_g show the proportionally constant and band gap energy, respectively. The plot of $(\alpha h\nu)^2$ vs. $h\nu$ can be used for determining the band gap. The band gap of the synthesized nanolayered double hydroxide was calculated to be 2.2 eV by extrapolating the linear region of mentioned plot (Fig. S2) [21,32].

3.2. Comparison of adsorption, sonolysis and sonocatalysis in degradation of bordeaux red B

The degradation of bordeaux red B was investigated via various processes including adsorption, sonolysis and sonocatalysis. The values of the initial bordeaux red B concentration and sonocatalyst dosage were 0.02 and 0.5 g L^{-1} , respectively.

As it is obvious in Fig. 2, only 15% of bordeaux red B was removed via adsorption after 120 min of being stirred magnetically in the dark environment. The results demonstrated that only 19% of degradation efficiency can be obtained by sonolysis alone (in the absence of sonocatalyst) after 120 min of reaction time. The highest removal efficiency (90%) was obtained in the presence of zinc-iron nanolayered double hydroxide as sonocatalyst during 120 min. It should be noted that in order to eliminate the adsorption effect in

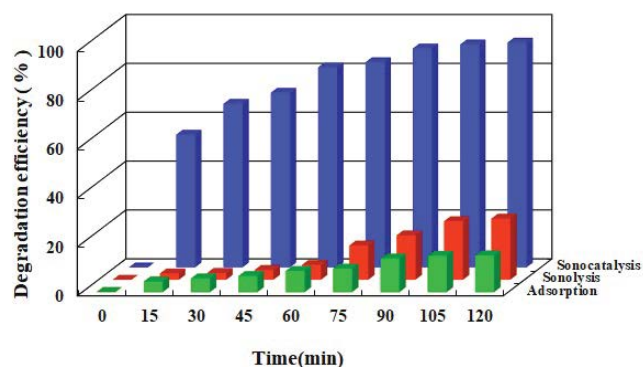


Fig. 2. Comparison of adsorption, sonolysis and sonocatalysis processes in degradation of bordeaux red B, experimental condition: [bordeaux red B] = 0.02 g L⁻¹, [sonocatalyst] = 0.5 g L⁻¹, power of ultrasonic = 300 W and pH = 6.

sonocatalysis process, the dye solution and sonocatalyst mixture was stirred for 30 min before ultrasonic irradiation in sonocatalysis processes.

3.3. Effects of different parameters on the sonocatalytic degradation of bordeaux red B

The dependence of the kinetic modeling of the sonocatalytic degradation on the sonocatalyst dosage and initial dye concentration was studied by performing two various series of experiments. The operational conditions are depicted in Table 2. The influence of the sonocatalyst concentration on the degradation efficiency and linear relationship of bordeaux red B degradation during sonocatalytic degradation process are represented in Fig. 3. As can be seen in Fig. 3(a), the results demonstrated that by increasing the sonocatalyst concentration from 0.1 g L⁻¹ concentration up to 0.5 g L⁻¹, the degradation efficiency was improved from 58% to 94% and then decreased after 120 min of sonocatalytic reaction. The increment of sonocatalyst dosage up to optimum amount increased the degradation efficiency by increasing the •OH radicals generation due to increasing the active reaction sites via providing great available surface area [33]. The decrement in degradation efficiency was observed at other values than optimum amount of sonocatalyst which can be attributed to aggregation of the sonocatalyst resulting in decreasing the number of the surface active sites [5,34]. In addition, Fig. 3(b) shows high correlation coefficient (R^2) for different sonocatalyst dosage in the range of 0.1–1 g L⁻¹, demonstrating that experimental data of bordeaux red B degradation with different sonocatalyst dosages can be well fitted with pseudo-first-order kinetic equation. The effect of

Table 2
Operational conditions of sonocatalytic degradation of bordeaux red B

Parameter	Range
Dye concentration (g L ⁻¹)	0.01–0.05
Sonocatalyst concentration (g L ⁻¹)	0.1–1
Ultrasonic power (W)	300

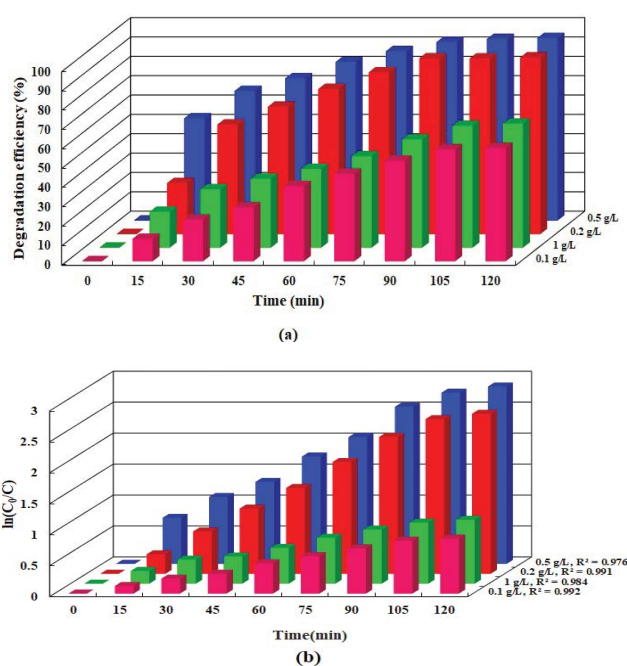


Fig. 3. (a) Effect of sonocatalyst concentration on the sonocatalytic degradation of bordeaux red B and (b) linear relationship of bordeaux red B degradation during sonocatalytic degradation process at different sonocatalyst dosage, experimental condition: [bordeaux red B] = 0.02 g L⁻¹, power of ultrasonic = 300 W and pH = 6.

the initial concentration of bordeaux red B on the degradation efficiency was studied, and the results are reported in Fig. 4. As can be seen in Fig. 4(a), by enhancing the initial bordeaux red B concentration from 0.01 to 0.05 g L⁻¹, the degradation efficiency diminished from 97% to 51%, after 120 min of sonocatalytic reaction time. By enhancing the number of dye molecules, the requirement for hydroxyl radicals for degradation of dye molecules enhances. Considering that the number of generated hydroxyl radicals is constant under the constant conditions, the degradation efficiency decreases by increasing dye concentration [35]. Moreover, the active sites of zinc-iron nanolayered double hydroxide as sonocatalyst can be occupied with molecules of dye at high concentration of dye which prevents the absorption of energy produced via cavitation phenomenon, resulting in a decline in degradation efficiency. High correlation coefficient ($R^2 \geq 0.989$) was resulted for different initial dye concentrations, indicating well-fitness of experimental data of bordeaux red B degradation with different initial dye concentration with pseudo-first-order kinetic equation (Fig. 4(b)) [6].

3.4. Mechanistic aspects of sonolysis and sonocatalytic degradation of bordeaux red B

The possible mechanisms for sonolytic and sonocatalytic degradation of bordeaux red B were proposed in Tables 3 and 4, respectively. Under ultrasonic waves in sonolysis and sonocatalytic degradation of organic compounds, microbubbles are produced, grow and implasively collapse. Reaction regions with high temperature (~5,000 K) and pressure

(~1,800 bar) in the aqueous solution which are generated from the collapse of the bubbles are considered as hot spots [36]. Three probable zones caused by sonochemical processes can be considered including inside of the bubbles, bubble–liquid interfacial region and liquid bulk. Due to the high radical concentration achieved by high temperature, gas–liquid interfacial region has been proposed to be the most effective zone for destruction of non-volatile and hydrophilic compounds [11,37].

In sonolysis, pyrolysis of water by hot spots generates hydroxyl and hydrogen radicals as shown in reaction 1 (Table 3) [38]. According to reaction 2, oxygen molecules can be converted to oxygen atoms by thermal dissociation. In reaction 3, $\cdot\text{OH}$ radicals can be produced through

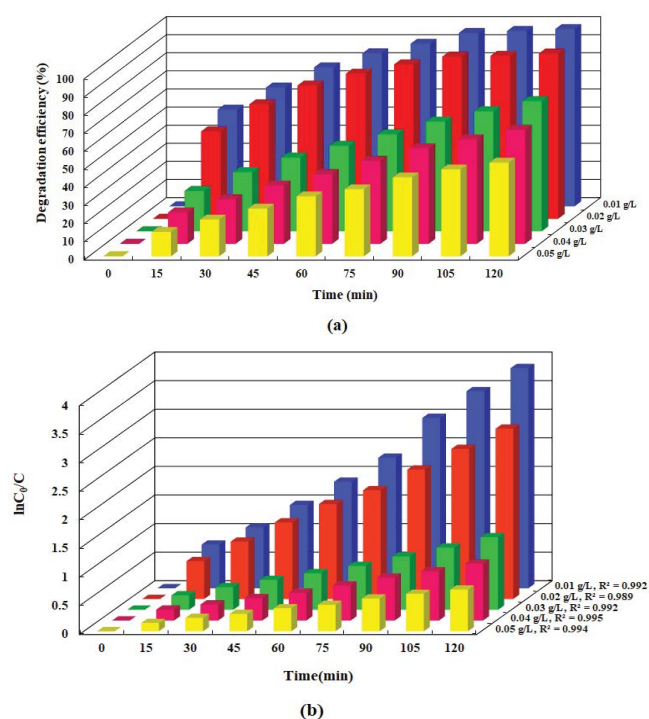


Fig. 4. (a) Effect of dye concentration on the sonocatalytic degradation of bordeaux red B and (b) linear relationship of bordeaux red B degradation during sonocatalytic degradation process at different bordeaux red B concentration, experimental condition: [sonocatalyst] = 0.5 g L⁻¹, power of ultrasonic = 300 W and pH = 6.

Table 3
Reactions involved in oxidation of bordeaux red B by sonochemical process

Reaction No.	Elementary reaction	Kinetic constant	Ref.
1	$\text{H}_2\text{O} + \text{Ultrasonic irradiation} \rightarrow \cdot\text{OH} + \text{H}\cdot$	k_1	[1,2]
2	$\text{O}_2 + \text{Ultrasonic irradiation} \rightarrow 2\text{O}\cdot$	k_2	[3]
3	$\text{O}\cdot + \text{H}_2\text{O} \rightarrow 2\cdot\text{OH}$	k_3	[3]
4	$\text{H}\cdot + \text{O}_2 \rightarrow \text{HO}_2\cdot$	$k_4 = 2.1 \times 10^{10} \text{M}^{-1}\text{S}^{-1}$	[1,2]
5	$\text{H}\cdot + \text{HO}_2\cdot \rightarrow \text{H}_2\text{O}_2$	$k_5 = 2.1 \times 10^{10} \text{M}^{-1}\text{S}^{-1}$	[3]
6	$\cdot\text{OH} + \text{H}_2\text{O}_2 \rightarrow \text{H}_2\text{O} + \text{HO}_2\cdot$	$k_6 = 2.7 \times 10^7 \text{M}^{-1}\text{S}^{-1}$	[1,2]
7	$\cdot\text{OH} + \text{Bordeaux red B} \rightarrow \text{Intermediate products}$	k_7	
8	$\cdot\text{OH} + \text{Intermediate products} \rightarrow \text{Degradation products}$	k_8	

the reaction of the formed oxygen atoms with water [39]. In addition, hydroperoxyl radicals ($\text{HO}_2\cdot$) can be produced by reacting O_2 molecules present in the vapor phase of the bubble with $\cdot\text{H}$ (reaction 4), the produced radical can be converted to hydrogen peroxide (reaction 5), which can scavenge hydroxyl radicals according to reaction 6 [40–42]. Organic compounds can be oxidized by generated $\cdot\text{OH}$ radicals (reactions 7 and 8) [43].

Degradation efficiency enhancement in the presence of sonocatalyst can be interpreted considering the sonoluminescence phenomenon. Sonoluminescence results by recombination of the free radicals produced within cavitation bubbles and includes the emission of light [38]. The emitted light which contains ultraviolet irradiation can excite the semiconductor applied as sonocatalyst, resulting in producing electron–hole pairs on the semiconductor (reaction 9, Table 4). [44,45]. A fraction of sonogenerated electron–hole pairs can be recombined via reaction 10. As shown by reaction 11, superoxide anion radicals can be formed by the reaction of electron acceptor species such as O_2 with sonogenerated electrons. By generating the electron–hole pairs on the surface of sonocatalyst, the water molecules and hydroxide ions adsorbed on sonocatalyst can react with generated holes and produce hydroxyl radicals (reactions 12 and 13). In addition to $\text{O}_2\cdot^-$ and $\cdot\text{OH}$, radicals of $\text{HO}_2\cdot$ and H_2O_2 species, which are powerful oxidant, can be generated according to the reactions 14 and 15, respectively [44]. As can be seen in reactions 17 and 18, hydroxyl radicals can degrade bordeaux red B molecules.

3.5. Development of a kinetic model using intrinsic elementary reactions

The intrinsic elementary reactions presented in Tables 3 and 4 were applied for developing a kinetic model. In order to develop an appropriate kinetic model, the following assumptions are expressed by considering the experimental conditions.

- Bulk solution which contains nanolayered double hydroxide as sonocatalyst is stirred magnetically in dark for 20 min to establish equilibrium conditions between bordeaux red B and sonocatalyst surface.
- The concentration of reactive species such as hydroxyl radicals, h^+ and e^- generated through sonocatalytic process is based on steady-state assumptions (SSA).
- The concentration of h^+ and e^- is equal.

Table 4
Reactions involved in oxidation of Bordeaux red B by sonocatalytic process

Reaction No.	Elementary reaction	Kinetic constant	Ref.
9	Semiconductor ZnFe – NLDH + ultrasonic irradiation → e ⁻ + h ⁺	k ₉	
10	e ⁻ + h ⁺ → heat	k ₁₀	[2]
11	e ⁻ + O ₂ → O ₂ ^{-•}	k ₁₁	
12	ZnFe – NLDH – H ₂ O + h ⁺ → ZnFe – NLDH – •OH + H ⁺	k ₁₂	[2]
13	ZnFe – NLDH – OH ⁻ + h ⁺ → ZnFe – NLDH – •OH	k ₁₃	[2]
14	ZnFe – NLDH – O ₂ ^{-•} + H ⁺ → ZnFe – NLDH – H ₂ O [•]	k ₁₄	[3]
15	ZnFe – NLDH – H ₂ O [•] + H ⁺ + e ⁻ → ZnFe – NLDH – H ₂ O ₂	k ₁₅	[3]
16	ZnFe – NLDH – H ₂ O ₂ + e ⁻ → ZnFe – NLDH – •OH + OH ⁻	k ₁₆	[3]
17	ZnFe – NLDH – •OH + Bordeaux red B → intermediate products	k ₁₇	
18	ZnFe – NLDH – •OH + intermediate → degradation products	k ₁₈	

Since the concentration of dissolved oxygen molecules in the solution bulk is low, reactions 2–5, 11 and also reactions 14–16 can be neglected. In addition, the influences of degassing by ultrasonic waves have intensified this phenomenon [46].

According to the expressed assumptions, the overall reaction rate for the sonocatalytic degradation of bordeaux red B can be described in Eq. (5):

$$r_{\text{tot}} = -\frac{1}{V} \times \frac{dN}{dt} = -\frac{dc}{dt} = k_{\text{hetero.sono}} [\bullet\text{OH}] [\text{Dye}] + k_{\text{hetero.cat}} [\bullet\text{OH}] [\text{Dye}] \quad (5)$$

In which r_{tot} , N , V , t , $K_{\text{hetero.sono}}$ and $K_{\text{hetero.cat}}$ represent the total reaction rate, moles of bordeaux red B, reaction volume, reaction time and second-order kinetic constants for the sonolysis and sonocatalytic reactions, respectively. By considering two second-order kinetic expressions given in Eq. (5), the concentration of •OH radicals by applying SSA can be calculated individually for each expression. Eq. (6) was used for determination of the total concentration of •OH radicals:

$$\frac{d[\bullet\text{OH}]_{\text{interface}}}{dt} = k_{\text{us}} [\text{H}_2\text{O}] + 2k_3 [\text{O}^*] [\text{H}_2\text{O}] - k_6 [\bullet\text{OH}] [\text{H}_2\text{O}_2] - k_7 [\bullet\text{OH}] [\text{Dye}]_{\text{interface}} - k_8 [\bullet\text{OH}] [\text{IP}]_{\text{interface}} \approx 0 \quad (6)$$

where k_{us} is the kinetic constant of reaction 1, and IP represents the intermediate products. Due to the aforementioned reason, $k_6 [\bullet\text{OH}] [\text{H}_2\text{O}_2]$ and $k_3 [\text{O}^*] [\text{H}_2\text{O}]$ expressions can be neglected in Eq. (6). Since determining the concentrations of $[\text{IP}]_{\text{interface}}$ and $[\text{Dye}]_{\text{interface}}$ is difficult, by considering Eqs. (7) and (6) can be modified to Eq. (8).

$$[\text{Dye}]_{\text{interface}} + [\text{IP}]_{\text{interface}} = [\text{Dye}]_{\text{tot-interface}} \quad (7)$$

$$k_7 [\text{Dye}]_{\text{interface}} + k_8 [\text{IP}]_{\text{interface}} = k_7 ([\text{Dye}]_{\text{tot-interface}} - [\text{IP}]_{\text{interface}}) + k_8 ([\text{Dye}]_{\text{tot-interface}} - [\text{Dye}]_{\text{interface}}) = (k_7 + k_8) [\text{Dye}]_{\text{tot-interface}} - k_7 [\text{IP}]_{\text{interface}} - k_8 [\text{Dye}]_{\text{interface}} \approx (k_7 + k_8) [\text{Dye}]_{\text{tot-interface}} \quad (8)$$

Because of the constant concentration of water in the bulk, Eq. (6) can be reformed to Eq. (9) by substituting k'_{us} instead of $k_{\text{us}} [\text{H}_2\text{O}]$.

$$[\bullet\text{OH}]_{\text{interface}} = \frac{k'_{\text{us}}}{(k_7 + k_8)} [\text{Dye}]_{\text{tot-interface}} \quad (9)$$

Based on the steady-state approximation, the total concentration of hydroxyl radicals adsorbed on the surface of sonocatalyst can be determined:

$$\frac{d[\bullet\text{OH}]_{\text{ads}}}{dt} = k_{12} [\text{H}_2\text{O}]_{\text{ads}} [h^+] + k_{13} [\text{OH}^-]_{\text{ads}} [h^+] + k_{16} [\text{H}_2\text{O}_2]_{\text{ads}} [e^-] - k_{17} [\bullet\text{OH}]_{\text{ads}} [\text{Dye}]_{\text{ads}} - k_{18} [\bullet\text{OH}]_{\text{ads}} [\text{IP}]_{\text{ads}} = 0 \quad (10)$$

If it supposed that the large amount of •OH radicals is produced by adsorbed water molecules, because of the vicinity of natural pH of bordeaux red B (pH = 6) to the neutral pH governing in the experiments, the following assumption is found: $k_{12} [\text{H}_2\text{O}]_{\text{ads}} [h^+] \gg k_{13} [\text{OH}^-]_{\text{ads}} [h^+]$.

Due to the constant solvent concentration, $k_{12} [\text{H}_2\text{O}]$ is equal to k'_{12} . Besides, $k_{16} [\text{H}_2\text{O}_2]_{\text{ads}} [e^-]$ can be neglected because of the low concentration of H₂O₂ resulted by low concentration of dissolved O₂. Consequently, Eq. (10) can be rearranged to Eq. (11):

$$[\bullet\text{OH}]_{\text{ads}} = \frac{k_{12} [h^+]}{k_{17} [\text{Dye}]_{\text{ads}} + k_{18} [\text{IP}]_{\text{ads}}} \quad (11)$$

$$[\text{Dye}]_{\text{ads}} + [\text{IP}]_{\text{ads}} = [\text{Dye}]_{\text{tot-ads}} \quad (12)$$

$$k_{17} [\text{Dye}]_{\text{ads}} + k_{18} [\text{IP}]_{\text{ads}} = k_{17} ([\text{Dye}]_{\text{tot-ads}} - [\text{IP}]_{\text{ads}}) + k_{18} ([\text{Dye}]_{\text{tot-ads}} - [\text{Dye}]_{\text{ads}}) = (k_{17} + k_{18}) [\text{Dye}]_{\text{tot-ads}} - k_{17} [\text{IP}]_{\text{ads}} - k_{18} [\text{Dye}]_{\text{ads}} \approx (k_{17} + k_{18}) [\text{Dye}]_{\text{tot-interface}} \quad (13)$$

By including Eq. (13) in Eq. (11), Eq. (14) is achieved:

$$[\bullet\text{OH}]_{\text{ads}} = \frac{k'_{12} [h^+]}{(k_{17} + k_{18}) - [\text{Dye}]_{\text{tot-ads}}} \quad (14)$$

The concentration of h^+ induced by sonocatalytic process can be determined using Eq. (15) by applying SSA:

$$\frac{d[h^+]}{dt} = k_9 I_{us} [\text{NLDH}] - k_{10} [h^+]^2 - k_{12} [\text{H}_2\text{O}]_{\text{ads}} [h^+] - k_{13} [\text{OH}^-]_{\text{ads}} [h^+] = 0 \quad (15)$$

Since the power of the applied ultrasonic irradiation was constant during the experiments, $k_9 I_{us} [\text{NLDH}]$ can be rewritten as $k'_9 [\text{NLDH}]$. Considering this fact that recombination rate of generated h^+ and e^- is effectively more than trapping h^+ by water molecules and considering that $k_{12} [\text{H}_2\text{O}]_{\text{ads}} [h^+] \gg k_{13} [\text{OH}^-]_{\text{ads}} [h^+]$, Eq. (15) can be modified to Eq. (16) [47].

$$[h^+] = \left(\frac{k'_9 [\text{NLDH}]}{k_{10}} \right)^{0.5} \quad (16)$$

Based on SSA, concentration of the adsorbed $\cdot\text{OH}$ radicals can be determined through including Eq. (16) in Eq. (15) which leads to Eq. (17):

$$[\cdot\text{OH}]_{\text{ads}} = \frac{k'_{12} \left(\frac{k'_9 [\text{NLDH}]}{k_{10}} \right)^{0.5}}{\left((k_{17} - k_{18}) [\text{Dye}]_{\text{tot-ads}} \right)} \quad (17)$$

By combining Eq. (9) and Eq. (17), the total destruction rate expression for sonocatalytic degradation of bordeaux red B can be represented by Eq. (18):

$$r_{\text{tot}} = k_{\text{hetero.sono}} \frac{k'_{us}}{(k_7 + k_8) [\text{Dye}]_{\text{tot-interface}}} [\text{Dye}] + k_{\text{hetero.cat}} \frac{k'_{12} \left(\frac{k'_9 [\text{NLDH}]}{k_{10}} \right)^{0.5}}{(k_{17} + k_{18}) [\text{Dye}]_{\text{tot-ads}}} [\text{Dye}] \quad (18)$$

By considering Eq. (18), k_{app} can be determined as follows:

$$k_{\text{app}} = k_{\text{hetero.sono}} \frac{k'_{us}}{(k_7 + k_8) [\text{Dye}]_{\text{tot-inter}}} + k_{\text{hetero.cat}} \frac{k'_{12} \left(\frac{k'_9 [\text{NLDH}]}{k_{10}} \right)^{0.5}}{(k_{17} + k_{18}) [\text{Dye}]_{\text{tot-ads}}} \quad (19)$$

Eq. (20) illustrates a pseudo-first order rate reaction with the respect to the bordeaux red B concentration.

$$k_{\text{app}} = \frac{k_{\text{hetero.sono}} k'_{us} y (k_{17} + k_{18}) + k_{\text{hetero.cat}} k'_{12} \left(\frac{k'_9 [\text{NLDH}]^{0.5}}{k_{10}} \right) x (k_7 + k_8)}{(k_7 + k_8) xy (k_{17} + k_{18}) [\text{Dye}]_0} \quad (20)$$

In order to simplify, Eqs. (20)–(25) are considered to develop Eq. (27).

$$[\text{Dye}]_{\text{tot-interface}} = x [\text{Dye}]_0 \quad (21)$$

$$[\text{Dye}]_{\text{tot-ads}} = y [\text{Dye}]_0 \quad (22)$$

$$\alpha = k_{\text{hetero.sono}} k'_{us} y (k_{17} + k_{18}) \quad (23)$$

$$\beta = k_{\text{hetero.cat}} k'_{12} x \left(\frac{k'_9}{k_{10}} \right)^{0.5} (k_7 + k_8) \quad (24)$$

$$\gamma = (k_7 + k_8) xy (k_{17} + k_{18}) \quad (25)$$

$$k_{\text{app}} = \frac{\alpha + \beta [\text{NLDH}]^{0.5}}{\gamma [\text{Dye}]_0} \quad (26)$$

Eq. (26) reveals that the degradation rate constant is a function of sonocatalyst concentration and initial concentration of bordeaux red B. A least square curve fit method by Matlab a2013 was applied for calculating the values of α , β and γ constants. The results are reported in Table 5.

Finally, the expression for predicting the degradation efficiency of bordeaux red B by considering the pseudo-first-order rate equation can be ascribed by Eq. (27).

$$\text{Decolorization efficiency}_{\text{predicted}} (\%) = 1 - \exp \left(- \left(\frac{\alpha + \beta [\text{NLDH}]^{0.5}}{\gamma [\text{Dye}]_0} \right) \times t \right) \quad (27)$$

To evaluate the developed kinetic model, the predicted bordeaux red B degradation efficiency determined from Eq. (27) was plotted in respect to the experimental bordeaux red B degradation efficiency (Fig. 5). The value of 0.975 for R^2 implies a significant correlation among the experimental bordeaux red B degradation efficiency and the values

Table 5

Calculated constant values by least square method for degradation of bordeaux red B in the presence of zinc-iron nanolayered double hydroxide

[Dye] ₀ (g L ⁻¹)	[Sonocatalyst] (g L ⁻¹)	Kinetic model	Parameter	Value
0.01–0.05	0.5	$k_{\text{app}} = \frac{\alpha + \beta [\text{ZnFe-NLDH}]^{1/2}}{\gamma [\text{DYE}]_0}$	α	$5.53 \times 10^{-2} \text{ L g}^{-1} \cdot \text{s}^3$
	β		$0.158 \text{ L}^{1.5} \text{ g}^{-1.5} \cdot \text{s}^3$	
	γ		$416 \times 10^{-3} \text{ L}^2 \text{ g}^{-2} \cdot \text{s}^2$	
0.02	0.1–1.0		α	$4.97 \times 10^{-2} \text{ L g}^{-1} \cdot \text{s}^3$
			β	$0.169 \text{ L}^{1.5} \text{ g}^{-1.5} \cdot \text{s}^3$
			γ	$359 \times 10^{-3} \text{ L}^2 \text{ g}^{-2} \cdot \text{s}^2$

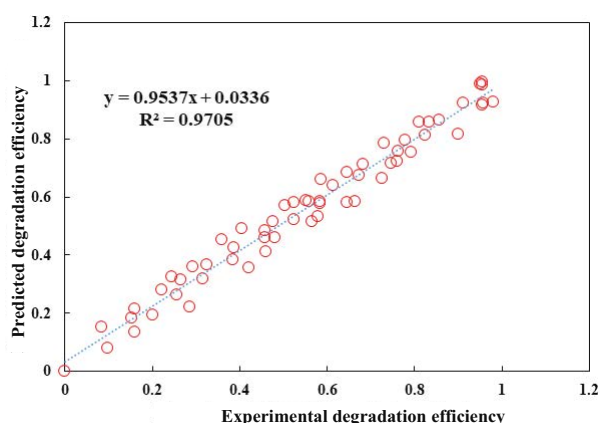


Fig. 5. Predicted degradation efficiency vs. experimental degradation efficiency with those calculated via developed kinetic model, experimental condition: [bordeaux red B] = 0.02 g L⁻¹, [sonocatalyst] = 0.5 g L⁻¹, power of ultrasonic = 300 W.

of degradation efficiency predicted by Eq. (27). The results demonstrated that the mechanism proposed for reaction and also the assumption used for developing the model are valid.

4. Conclusions

The sonocatalytic degradation of bordeaux red B in the presence of zinc-iron nanolayered double hydroxide was modeled based on the intrinsic elementary reactions. Convenient co-precipitation method was applied for preparation of zinc-iron nanolayered double hydroxide. The SEM analysis showed that the mean diameter of the nanosheets in synthesized nanolayered double hydroxide is about 32.5 nm. The XRD patterns revealed the preparation of nanosheets with average crystallite size of 13 nm. The effects of the sonocatalyst concentration and initial bordeaux red B concentration were investigated on the sonocatalytic degradation efficiency of bordeaux red B. A novel kinetic model was developed based on intrinsic elementary reactions to predict the removal efficiency of bordeaux red B. The developed kinetic model completely indicates the influence of sonocatalyst concentration and initial bordeaux red B concentration on the degradation apparent rate constant. High R^2 value (0.975) confirmed a significant correlation between the experimental bordeaux red B degradation efficiency and the values predicted by as-developed kinetic model. It can be concluded that the considered assumptions and intrinsic sonolysis and sonocatalysis reactions applied to propose the kinetic model are valid.

Acknowledgments

The authors would like to sincerely thank the University of Tabriz (Iran) for providing all of the support.

References

- [1] A. Khataee, R.D.C. Soltani, A. Karimi, S.W. Joo, Sonocatalytic degradation of a textile dye over Gd-doped ZnO nanoparticles synthesized through sonochemical process, *Ultrason. Sonochem.*, 23 (2015) 219–230.
- [2] R.D.C. Soltani, A. Khataee, M. Mashayekhi, Photocatalytic degradation of a textile dye in aqueous phase over ZnO nanoparticles embedded in biosilica nanobiostructure, *Desal. Wat. Treat.*, 57 (2016) 13494–13504.
- [3] R.D.C. Soltani, A. Rezaee, A. Khataee, Combination of carbon black–ZnO/UV process with an electrochemical process equipped with a carbon black–PTFE-coated gas-diffusion cathode for removal of a textile dye, *Ind. Eng. Chem. Res.*, 52 (2013) 14133–14142.
- [4] A. Ghalajkhani, M. Haghghi, M. Shabani, Efficient photocatalytic degradation of methylene blue in aqueous solution over flowerlike nanostructured MoS₂-FeZnO staggered heterojunction under simulated solar-light irradiation, *J. Photochem. Photobiol., A*, 359 (2018) 145–156.
- [5] N. Ertugay, F.N. Acar, The degradation of Direct Blue 71 by sono, photo and sonophotocatalytic oxidation in the presence of ZnO nanocatalyst, *Appl. Surf. Sci.*, 318 (2014) 121–126.
- [6] A. Hassani, R.D.C. Soltani, S. Karaca, A. Khataee, Preparation of montmorillonite–alginate nanobiocomposite for adsorption of a textile dye in aqueous phase: isotherm, kinetic and experimental design approaches, *J. Ind. Eng. Chem.*, 21 (2015) 1197–1207.
- [7] N. Ertugay, F.N. Acar, Sonocatalytic degradation of Direct Blue 71 azo dye at the presence zero-valent iron (ZVI), *Desal. Wat. Treat.*, 51 (2013) 7570–7576.
- [8] L. Song, C. Chen, S. Zhang, Q. Wei, Sonocatalytic degradation of amaranth catalyzed by La³⁺ doped TiO₂ under ultrasonic irradiation, *Ultrason. Sonochem.*, 18 (2011) 1057–1061.
- [9] N. Ghows, M.H. Entezari, Kinetic investigation on sonodegradation of Reactive Black 5 with core–shell nanocrystal, *Ultrason. Sonochem.*, 20 (2013) 386–394.
- [10] B. Neppolian, A. Bruno, C.L. Bianchi, M. Ashokkumar, Graphene oxide based Pt–TiO₂ photocatalyst: ultrasound assisted synthesis, characterization and catalytic efficiency, *Ultrason. Sonochem.*, 19 (2012) 9–15.
- [11] L. Zhu, Z.D. Meng, C.Y. Park, T. Ghosh, W.C. Oh, Characterization and relative sonocatalytic efficiencies of a new MWCNT and CdS modified TiO₂ catalysts and their application in the sonocatalytic degradation of rhodamine B, *Ultrason. Sonochem.*, 20 (2013) 478–484.
- [12] O. Yayapao, T. Thongtem, A. Phuruangrat, S. Thongtem, Sonochemical synthesis of Dy-doped ZnO nanostructures and their photocatalytic properties, *J. Alloys Compd.*, 576 (2013) 72–79.
- [13] S. Farhadi, F. Siadatnasab, Sonocatalytic degradation of organic pollutants by CdS nanoparticles hydrothermally prepared from cadmium (II) diethanoldithiocarbamate, *Desal. Wat. Treat.*, 66 (2017) 299–308.
- [14] J. Wang, Y. Guo, B. Liu, X. Jin, L. Liu, R. Xu, Y. Kong, B. Wang, Detection and analysis of reactive oxygen species (ROS) generated by nano-sized TiO₂ powder under ultrasonic irradiation and application in sonocatalytic degradation of organic dyes, *Ultrason. Sonochem.*, 18 (2011) 177–183.
- [15] A.I. Khan, A. Ragavan, B. Fong, C. Markland, M. O'Brien, T.G. Dunbar, G.R. Williams, D. O'Hare, Recent developments in the use of layered double hydroxides as host materials for the storage and triggered release of functional anions, *Ind. Eng. Chem. Res.*, 48 (2009) 10196–10205.
- [16] F. Li, X. Duan, Applications of Layered Double Hydroxides, in: *Layered Double Hydroxides*, Springer-Verlag Berlin Heidelberg, 2006, pp. 193–223.
- [17] J. He, M. Wei, B. Li, Y. Kang, D. Evans, X. Duan, Preparation of Layered Double Hydroxides, X. Duan, D.G. Evans, Eds., *Layered Double Hydroxides. Structure and Bonding*, Springer, Berlin Heidelberg, 2006, pp. 89–119.
- [18] F.L. Theiss, M.J. Sear-Hall, S.J. Palmer, R.L. Frost, Zinc aluminium layered double hydroxides for the removal of iodine and iodide from aqueous solutions, *Desal. Wat. Treat.*, 39 (2012) 166–175.
- [19] G. Xie, K. Zhang, H. Fang, B. Guo, R. Wang, H. Yan, L. Fang, J.R. Gong, A photoelectrochemical investigation on the synergetic effect between CdS and reduced graphene oxide for solar-energy conversion, *Chem. Asian J.*, 8 (2013) 2395–2400.
- [20] S.J. Xia, Z.M. Ni, Q. Xu, B.X. Hu, J. Hu, Layered double hydroxides as supports for intercalation and sustained release of antihypertensive drugs, *J. Solid State Chem.*, 181 (2008) 2610–2619.
- [21] S.J. Xia, F.X. Liu, Z.M. Ni, J.L. Xue, P.P. Qian, Layered double hydroxides as efficient photocatalysts for visible-light degradation of Rhodamine B, *J. Colloid Interface Sci.*, 405 (2013) 195–200.

- [22] J. Wang, Z. Jiang, L. Zhang, P. Kang, Y. Xie, Y. Lv, R. Xu, X. Zhang, Sonocatalytic degradation of some dyestuffs and comparison of catalytic activities of nano-sized TiO_2 , nano-sized ZnO and composite TiO_2/ZnO powders under ultrasonic irradiation, *Ultrason. Sonochem.*, 16 (2009) 225–231.
- [23] S.N. Nam, S.K. Han, J.W. Kang, H. Choi, Kinetics and mechanisms of the sonolytic destruction of non-volatile organic compounds: investigation of the sonochemical reaction zone using several OH monitoring techniques, *Ultrason. Sonochem.*, 10 (2003) 139–147.
- [24] N. Serpone, R. Terzian, H. Hidaka, E. Pelizzetti, Ultrasonic induced dehalogenation and oxidation of 2-, 3-, and 4-chlorophenol in air-equilibrated aqueous media. Similarities with irradiated semiconductor particulates, *J. Phys. Chem.*, 98 (1994) 2634–2640.
- [25] Y.L. Pang, A.Z. Abdullah, Comparative study on the process behavior and reaction kinetics in sonocatalytic degradation of organic dyes by powder and nanotubes TiO_2 , *Ultrason. Sonochem.*, 19 (2012) 642–651.
- [26] A. Khataee, M. Fathinia, T.S. Rad, Kinetic modeling of nalidixic acid degradation by clinoptilolite nanorod-catalyzed ozonation process, *RSC Adv.*, 6 (2016) 44371–44382.
- [27] A. Amani-Ghadim, M.S. Dorraji, Modeling of photocatalytic process on synthesized ZnO nanoparticles: kinetic model development and artificial neural networks, *Appl. Catal., B*, 163 (2015) 539–546.
- [28] M.S. Dorraji, A. Amani-Ghadim, M. Rasoulifard, S. Taherkhani, H. Daneshvar, The role of carbon nanotube in zinc stannate photocatalytic performance improvement: experimental and kinetic evidences, *Appl. Catal., B*, 205 (2017) 559–568.
- [29] L. Xu, W. Chu, N. Graham, Sonophotolytic degradation of dimethyl phthalate without catalyst: analysis of the synergistic effect and modeling, *Water Res.*, 47 (2013) 1996–2004.
- [30] H. Zhang, X. Wen, Y. Wang, Synthesis and characterization of sulfate and dodecylbenzenesulfonate intercalated zinc-iron layered double hydroxides by one-step coprecipitation route, *J. Solid State Chem.*, 180 (2007) 1636–1647.
- [31] A. Patterson, The Scherrer formula for X-ray particle size determination, *Phys. Rev.*, 56 (1939) 978.
- [32] K. Parida, L. Mohapatra, Carbonate intercalated Zn/Fe layered double hydroxide: a novel photocatalyst for the enhanced photo degradation of azo dyes, *Chem. Eng. J.*, 179 (2012) 131–139.
- [33] T. Ghosh, K. Ullah, V. Nikam, C.Y. Park, Z.D. Meng, W.C. Oh, The characteristic study and sonocatalytic performance of CdSe-graphene as catalyst in the degradation of azo dyes in aqueous solution under dark conditions, *Ultrason. Sonochem.*, 20 (2013) 768–776.
- [34] Y.L. Pang, A.Z. Abdullah, S. Bhatia, Review on sonochemical methods in the presence of catalysts and chemical additives for treatment of organic pollutants in wastewater, *Desalination*, 277 (2011) 1–14.
- [35] B. Vahid, A. Khataee, Photoassisted electrochemical recirculation system with boron-doped diamond anode and carbon nanotubes containing cathode for degradation of a model azo dye, *Electrochim. Acta*, 88 (2013) 614–620.
- [36] A. Hassani, A. Khataee, S. Karaca, C. Karaca, P. Gholami, Sonocatalytic degradation of ciprofloxacin using synthesized TiO_2 nanoparticles on montmorillonite, *Ultrason. Sonochem.*, 35 (2017) 251–262.
- [37] Y.T. Didenko, W.B. McNamara, K.S. Suslick, Hot spot conditions during cavitation in water, *J. Am. Chem. Soc.*, 121 (1999) 5817–5818.
- [38] A. Khataee, S. Saadi, M. Safarpour, S.W. Joo, Sonocatalytic performance of Er-doped ZnO for degradation of a textile dye, *Ultrason. Sonochem.*, 27 (2015) 379–388.
- [39] B. Ervens, S. Gligorovski, H. Herrmann, Temperature-dependent rate constants for hydroxyl radical reactions with organic compounds in aqueous solutions, *Phys. Chem. Chem. Phys.*, 5 (2003) 1811–1824.
- [40] Y. Meng, X. Huang, Y. Wu, X. Wang, Y. Qian, Kinetic study and modeling on photocatalytic degradation of par-chlorobenzoate at different light intensities, *Environ. Pollut.*, 117 (2002) 307–313.
- [41] A. Khataee, M. Fathinia, S. Aber, Kinetic modeling of liquid phase photocatalysis on supported TiO_2 nanoparticles in a rectangular flat-plate photoreactor, *Ind. Eng. Chem. Res.*, 49 (2010) 12358–12364.
- [42] R. Vinu, G. Madras, Kinetics of sonophotocatalytic degradation of anionic dyes with nano- TiO_2 , *Environ. Sci. Technol.*, 43 (2008) 473–479.
- [43] C.H. Fischer, E.J. Hart, A. Henglein, Hydrogen/deuterium isotope exchange in the hydrogen deuteride-water system under the influence of ultrasound, *J. Phys. Chem.*, 90 (1986) 3059–3060.
- [44] A. Khataee, S. Saadi, B. Vahid, S.W. Joo, B.-K. Min, Sonocatalytic degradation of Acid Blue 92 using sonochemically prepared samarium doped zinc oxide nanostructures, *Ultrason. Sonochem.*, 29 (2016) 27–38.
- [45] J. Wang, T. Ma, Z. Zhang, X. Zhang, Y. Jiang, Z. Pan, Preparation of high active nanometer TiO_2 sonocatalyst by partial transition crystal in hydrogen peroxide solution under ultrasonic irradiation, *Catal. Commun.*, 8 (2007) 118–122.
- [46] T.J. Mason, A. Tiehm, *Advances in Sonochemistry: Ultrasound in Environmental Protection*, Elsevier, JAI press, UK, 2001.
- [47] G. Rothenberger, J. Moser, M. Graetzel, N. Serpone, D.K. Sharma, Charge carrier trapping and recombination dynamics in small semiconductor particles, *J. Am. Chem. Soc.*, 107 (1985) 8054–8059.

Supplementary Information

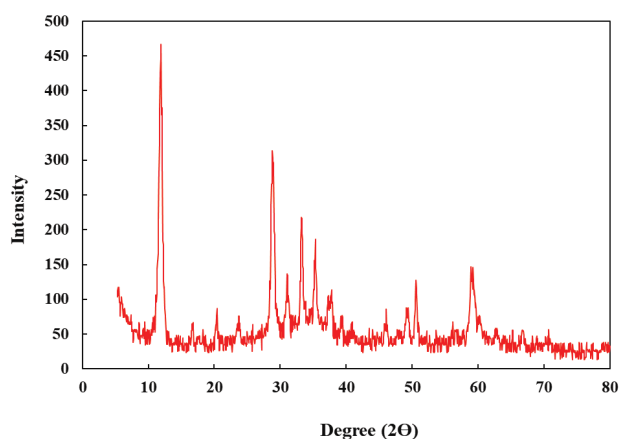


Fig. S1. XRD pattern of zinc-iron nanolayered double hydroxide.

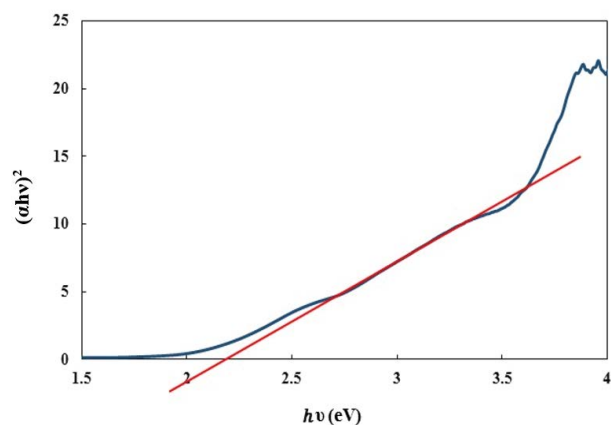


Fig. S2. UV-Vis diffuse reflectance spectrum of zinc-iron nanolayered double hydroxide.